Effects of Atmospheric Uncertainties On Sonic Boom Perceived Level

Article *in* Journal of Fluids Engineering · January 2021

DOI: 10.1115/1.4049688

CITATIONS
0

READS
12

3 authors:

Sohail R Reddy
Naval Postgraduate School
34 PUBLICATIONS **227** CITATIONS
SEE PROFILE

Janhavi Chitale
Florida International University
3 PUBLICATIONS **7** CITATIONS
SEE PROFILE

George S Dulikravich
Florida International University
383 PUBLICATIONS **3,843** CITATIONS
SEE PROFILE

Sohail R. Reddy[1,2]
Department of Mechanical and Materials Engineering,
MAIDROC Laboratory,
Florida International University,
Miami, FL 33174
e-mail: sredd001@fiu.edu

Janhavi Chitale
Department of Mechanical and Materials Engineering,
MAIDROC Laboratory,
Florida International University,
Miami, FL 33174
e-mail: jchit002@fiu.edu

George S. Dulikravich
Department of Mechanical and Materials Engineering,
MAIDROC Laboratory,
Florida International University,
Miami, FL 33174
e-mail: dulikrav@fiu.edu

Effects of Atmospheric Uncertainties on Sonic Boom Perceived Level

This work quantifies the uncertainty in Stevens Mark VII Perceived Level of sonic booms due to uncertainties in atmospheric profiles. The influence of temperature, humidity, and wind profiles, at six cities around the globe, on the sonic boom loudness is calculated. The flow field around an aircraft was obtained by solving the three-dimensional (3D), compressible Euler equations using the UNS3D solver. The near-field pressure signature is then propagated through the atmosphere by solving the augmented Burgers equation using the sBOOM solver. The uncertainty is modeled using a nonintrusive polynomial chaos approach. A sensitivity analysis is performed to identify the altitude range and the atmospheric variable to which the Perceived Level is most sensitive. It was shown that the Perceived Level is not sensitive to any particular altitude but rather the atmospheric profiles. It was also seen that the Perceived Level is highly sensitive to humidity and temperature profiles and less sensitive to the wind profiles. [DOI: 10.1115/1.4049688]

1 Introduction

Since the advent of supersonic flight, much effort has been dedicated to achieve a quieter flight. Prather et al. [1] presents current methods for operating supersonic transport (SST), which include limiting supersonic flights to specific corridors over land. Recent efforts have demonstrated the possibility of quieter supersonic flight [2], which has spawned multiple research efforts [3,4] toward lessening the negative impacts of sonic booms. While there were several optimization studies [5–7] that have been performed to design a low-boom supersonic aircraft, only one publicly available effort [8] has been made to design a robust low-boom aircraft considering impacts from effects of uncertainty in many atmospheric profiles on its sonic boom level. It is well known that the atmospheric conditions significantly influence the sonic boom propagation and the Perceived Level (PL) at the ground level. Little effort has been dedicated toward quantifying the uncertainty in PL due to atmospheric uncertainties.

Previous work of West et al. [9] investigated the uncertainty in the near-field and ground noise signature due to aleatory and epistemic uncertainty. Their work developed a computationally efficient framework for uncertainty quantification and sensitivity analysis. Fujino et al. [10] investigated the effects of atmospheric conditions on the peak pressure of the ground signature. However, their atmospheric data only considered the atmospheric profiles at three different times on a single day. Shimoyama et al. [11] and Jeong et al. [12] used polynomial chaos to compute the uncertainty in the pressure signature due to temperature, humidity, and wind profiles. Their study only considered the atmospheric profile at the Esrange Space Center between 2000 and 2009. Their research does not however provide numerical values of uncertainty, and comment only on the pressure signature and not the Perceived Level. Previous investigations in this field do not provide a quantifiable measure of the uncertainty in loudness. This study not only quantifies the uncertainty in sonic boom PL but also quantifies the extent to which each atmospheric variable influences the sonic boom loudness.

This study addresses these issues by considering Stevens Mark VII Perceived Level [13–15], which has been shown to correlate with human perception of sonic boom. It should also be mentioned that previous works only considered and drew their conclusions from the atmospheric conditions at one location. The atmospheric profiles used are also from relatively diverse climates and relatively recent. The atmospheric profiles during the year 2017 from six different cities from around globe are considered. The augmented Burgers equation is solved to propagate the near-field pressure wave to the ground using NASA's sBOOM solver [16]. A nonintrusive polynomial chaos approach is used to propagate the uncertainty through the system. The uncertainty in undertrack PL due to uncertainties in temperature, relative humidity, x-directional winds, and y-directional winds are quantified for an aircraft heading east, in the positive x direction. The sensitivity of PL to the atmospheric variables within an altitude range is also studied. Results show that the PL is most sensitive to humidity followed by temperature and x-directional winds. It is not sensitive to y-directional winds. It should be noted that the aircraft was assumed to be traveling in an easterly direction, where east and south are in the x and y direction, respectively. It is also shown that the atmospheric variables have more influence in a particular geographic region than another. This is due to the large variation in the atmospheric profile from one region to another. In previous studies, it was shown that the wind direction and velocity have negligible effect on the sonic boom loudness. In this work, however, it was seen that in certain cities, they are equally as important as temperature.

2 Analysis Framework

This section presents the framework and methodologies used to perform the sensitivity analysis and uncertainty quantification. It also presents the dataset used to obtain the atmospheric profiles and the near-field pressure waveform.

2.1 Fluid Dynamics Model. The velocity and pressure field near the aircraft was obtained using a cell-centered finite volume solver, UNS3D, developed at Texas A&M University [17]. Due to the high flight Reynolds number expected, the flow was assumed to be inviscid. The UNS3D solver was used to solve the

[1]Corresponding author.
[2]Present address: Department of Applied Mathematics, Naval Postgraduate School, Monterey, CA 93943.

Contributed by the Fluids Engineering Division of ASME for publication in the Journal of Fluids Engineering. Manuscript received March 12, 2020; final manuscript received December 31, 2020; published online February 8, 2021. Assoc. Editor: Elias Balaras.

three-dimensional (3D), steady-state, compressible Euler equations. The mass, momentum, and energy balance in the Euler system of equations are given as

$$\frac{\partial \rho}{\partial t} + \nabla \cdot (\rho \mathbf{u}) = 0 \tag{1}$$

$$\frac{\partial \rho \mathbf{u}}{\partial t} + \nabla \cdot \left(\rho \mathbf{u}\mathbf{u}^T\right) + \nabla p = 0 \tag{2}$$

$$\frac{\partial E}{\partial t} + \nabla \cdot (\mathbf{u}(E+p)) = 0 \tag{3}$$

where ρ, $\mathbf{u}$, p, T are the density, velocity, pressure, and temperature, $E = \rho e + \frac{1}{2}\rho u^2$ is the total energy per unit volume and is composed of the kinetic energy per unit volume ($\frac{1}{2}\rho u^2$) and the internal energy per unit volume (ρe). Here, e is the internal energy per unit mass.

The UNS3D solver computes the convective fluxes using Roe's approximate Riemann solver [18] in conjunction with Harten's entropy fix [19]. Second-order spatial accuracy was obtained using piecewise-linear reconstruction to obtain the left and right states (solution to the left and right side of the interface) when computing the convective fluxes. The Green-Gauss gradient reconstruction method [20] was used to compute the flow field gradients needed for piecewise-linear reconstruction. A steady-state solution was obtained by integrating the Euler system forward in pseudo-time using the General Minimal Residual Method (GMRES) [21]. Steady-state convergence was accelerated by employing local time-stepping.

2.2 Atmospheric Profiles. The atmospheric profiles used in this work were obtained from the National Oceanic and Atmospheric Administration (NOAA) [22,23] and are the weather balloon soundings from the Integrated Global Radiosonde Archive (IGRA). A total of six cities around the globe with diverse climates and weather profiles are considered: Miami, Las Vegas, Oslo, Glasgow, Mumbai, Shanghai, and a fictional city Combined is also considered. That is, the database of soundings for the "Combined" city contains the soundings from the remaining six cities. The distribution of variables for the Combined city is then obtained using this combined dataset of soundings. Only weather recordings at these cities during the year 2017, and only the variables that affect the sonic boom propagation, such as temperature, humidity, and winds, were considered. The soundings were often taken two to four times each day throughout the year. It should be mentioned that the database does not contain measurements for every day of the year, but is still sufficiently large.

Each atmospheric variable, at each city, was sampled throughout the year for a set of ten uniformly distributed altitude values. Preliminary studies showed that ten uniformly distributed points were sufficient to describe the complete atmospheric profile. The near-field and ground signatures were defined using 6340 and 40 000 points, respectively. The mean and standard deviation of each variable at each city as a function of altitude is shown in the Appendix. Finally, each atmospheric variable for a combined dataset of all cities was also sampled throughout the year at a set of 10 uniformly distributed altitudes. The uncertainty quantification is performed using the atmospheric profile at each city and the profile of the combined set, while the altitude sensitivity study is only performed using the profile of the combined set.

2.3 Sonic Boom Propagation. The sonic boom propagation in this work is performed using sBOOM [16] (Version 1 - NASA Ref. ID: LAR-18012-1). It solves the augmented Burgers equation [24], Eq. (4), in the time domain.

$$\frac{\partial p}{\partial x} = \frac{\beta p}{\rho_0 c_0^3}\frac{\partial p}{\partial t'} + \frac{\delta}{2c_0^3}\frac{\partial^2 p}{\partial t'^2} + \sum_v \frac{c_v'}{c_0^2}\int_{-\infty}^{t'} \frac{\partial^2 p}{\partial y^2} e^{-\frac{(t'-y)}{t_v}} dy \tag{4}$$

Here, β is the coefficient of nonlinearity, p is the pressure, ρ_0 is the ambient density, c_0 is the ambient speed of sound, t' is the retarded time coordinate, and δ is the diffusion parameter. The augmented Burgers equation accounts for nonlinearity, thermoviscous absorption, and any number of molecular relaxation phenomena (losses from O_2 and N_2) during the propagation of waveforms through the atmosphere.

Equation (4) can be converted to a dimensionless form

$$\frac{\partial P}{\partial \sigma} = P\frac{\partial P}{\partial \tau} + \frac{1}{\Gamma}\frac{\partial^2 P}{\partial \tau^2} + \sum_v C_v \frac{\partial^2/\partial\tau^2}{1+\theta_v(\partial/\partial\tau)}P - \frac{\partial A/\partial A}{2A}P + \frac{\partial(\rho_0 c_0)/\partial\sigma}{2\rho_0 c_0}P \tag{5}$$

where $P(\sigma,\tau) = p/p_0$, p_0 is the reference pressure and $\tau = \omega_0 t'$ is the dimensionless time. The nondimensional distance is given as $\sigma = x/\bar{x}$, where $\mathbf{x} = \rho_0 c_0^3/\beta\omega_0 p_0$ is the shock formation distance of a plane wave with an angular frequency ω_0. In Eq. (5), $\Gamma = 1/\alpha_0^{tv}\bar{x}$ is the dimensionless thermoviscous parameter, $\alpha_0^{tv} = \delta\omega_0^2/2c_0^3$ is the attenuation coefficient, $\theta_v = \omega_0 t_v$ is the dimensionless relaxation time parameter, $C_v = (m_v\tau_v\omega_0^2/2c_0)\bar{x}$ is the dimensionless dispersion parameter and m_v is the dispersion parameter. The reference pressure is obtained from the hydrostatic balance.

The sBOOM program solves this dimensionless version of the Burgers equation using an operator splitting approach. Given the temperature, relative humidity, and wind profiles, sBOOM computes the ground pressure signature. The Perceived Level, commonly referred to as PL or PLdB, of the ground pressure signature is then computed using the Stevens Mark VII procedure [13]. Sullivan [25] indicated that the PLdB metric is a more appropriate measure of loudness than the overpressure and the unweighted sound pressure level. The PLdB was computed using the open source package PyLdB [26]. The pressure wave that is propagated was obtained using the UNS3D solver from the NASA C25D geometry from the 2nd AIAA Sonic Boom Prediction Workshop [27]. It is the pressure signature created by a low-boom concept NASA C25D aircraft cruising at Mach 1.6 at an altitude of approximately 15600 meters. The ground reflection factor in sBOOM was held constant at 1.9. Each of the seven cities in this study was assumed to be at sea level (i.e., the ground elevation is held constant at 0 m). All atmospheric profiles were linearly extrapolated, from 200 m down to 0 m, in order to obtain their values at attitudes where measurements were not available. Since only the effects of atmospheric uncertainty are considered, all other parameters were held constant.

The augmented Burgers equation is a popular model for acoustic wave propagation. The model, however, does have some limitations. The viscous and nonlinear terms in the augmented Burgers equation are derived from one-dimensional form of the Navier–Stokes equations (NSE). In standard application of the NSE, the Stokes' hypothesis of bulk viscosity (μ_B) being zero is used [28]. This leads to the second coefficient of viscosity value of $\zeta = -\frac{2\mu}{3}$, where μ is the dynamic viscosity. Using the kinetic theory of gasses, this value was determined to be true for most of monatomic gasses. For air, the value of the bulk coefficient of viscosity is practically zero. Hence, Stokes hypothesis was assumed valid in these studies.

Gad-el-Hak [29] stated that in the case of flow of a polyatomic gas through a shock wave, the bulk viscosity is proportional to the longer relaxation time. This would lead to larger values for the second coefficient of viscosity. Dulikravich [30] and Dulikravich and Kennon [31] investigated the effects of the second coefficient of viscosity greater than the one given by the Stokes hypothesis and its effect viscosity on the strength of the shock and showed that a positive value of bulk viscosity lead to weaker shocks than the Rankine–Hugoniot shocks, which correspond to Stokes hypothesis only [30,31].

Landau and Lifshitz [28] showed that the intensity of the dissipative processes, and therefore the value of ζ depends on the

relation between the rate of compression/expansion and the relaxation time. Therefore, in the case of compression/expansion due to a sound wave, the second coefficient of viscosity might depend on the wave frequency. In traditional models, the second coefficient of viscosity is treated as a constant when in reality it is frequency-dependent [32]. The dependence of ζ on frequency is called its dispersion. Since the exact value of bulk viscosity for air is not known, it was assumed to be zero. Similarly, since the relationship between the second coefficient of viscosity and frequency is not known, it was assumed to be constant at $\zeta = -\frac{2\mu}{3}$. Since sBOOM solves the simplified model, these effects are not considered in the boom propagation.

2.4 Sensitivity Analysis Using Radial Enhanced Sampling for Uniformity. A popular screening type sensitivity analysis technique is Elementary Effects (EE) method [33–35]. It has been used in various areas of research ranging from the modeling of air-to-launch orbit separation [36], water quality [37], building energy analysis [38] to alloy solidification [39]. The EE method calculates local derivatives at points chosen by multivariate sampling in the input space to calculate global measurement of importance at a lower cost compared to other variance-based methods.

The elementary effects are calculated using Eq. (6) for a model with k input parameters, where Δ is the perturbation in the parameter i and r is the number of trajectories considered in sampling. Here, Δ is a multiple of $1/(n-1)$, usually set to $n/(2(n-1))$, where n is the number of levels along any input factor axis.

$$EE_i = \frac{y(x_1,\ldots,x_{i-1},x_i+\Delta,x_{i+1},\ldots,x_k) - y(x_1,\ldots,x_{i-1},x_i,x_{i+1},\ldots,x_k)}{\Delta} \tag{6}$$

A total of $r \times (k+1)$ model runs are required to calculate r elementary effects per parameter. The mean μ_i, mean of absolute values of elementary effects μ_i^* and standard deviation σ_i of the elementary effects for each parameter for all trajectories is calculated using Eqs. (7), (8), and (9), respectively.

$$\mu_i = \frac{1}{r}\sum_{j=1}^{r} EE_{i,j} \tag{7}$$

$$\mu_i^* = \frac{1}{r}\sum_{j=1}^{r} |EE_{i,j}| \tag{8}$$

$$\sigma_i = \sqrt{\frac{1}{r}\sum_{j=1}^{r} (EE_{i,j} - \mu_i)^2} \tag{9}$$

Parameters are plotted in $\mu^* - \sigma$ space to identify model behavior related to them and to segregate them into important and unimportant classes. The parameters closely clustered toward the origin are considered unimportant and the ones well-separated away from the origin are considered important. The parameters far from the origin and closer to the μ^* axis are considered to have high linear impact whereas the ones far from the origin and closer to the σ axis are considered to have high interaction effect [34]. Variables above the $\mu^* = \sigma$ line are considered to have some degree of interaction effect.

To avoid sparse representation of the input space and to improve quality of the screening process, a sampling strategy with the ability to produce a well-representative sample is of immense importance. The development in the sampling strategies for EE method has ranged from winding stair-case type trajectory-based strategies such as Optimized Trajectories (OT) [40], Sampling for Uniformity (SU) [41], and enhanced SU (eSU) [42] to radial or star shaped design-based strategies such as Radial Sampling [35] and Radial Quasi-Random Sampling [43]. Campolongo et al. [35] compared performance of radial and winding staircase type trajectories and concluded radial to be a better design. They suggested using Sobol quasi-random sequences to build a variable step - radial OAT sample to conduct EE analysis. Xiao et al. [43] demonstrated that radial design with fixed step size performed better than variable step type design. From the perspective of sample design, radial design has proven to be better than winding staircase design. Principle of uniformity states that the trajectories must be selected in such a way that the entire design space is covered. The sampling strategy used in this work, Radial enhanced Sampling for Uniformity (ReSU) combines the principle of uniformity with radial design.

2.5 Point-Collocation Nonintrusive Polynomial Chaos Expansion. In recent works, polynomial chaos expansion (PCE) has been the preferred method for quantifying uncertainty in a system over other methods such as Monte Carlo sampling [44–47]. The PCE approach decouples the system response, which is a function of a deterministic parameter D, and a stochastic parameter ξ, into a deterministic component and a stochastic component, Eq. (10),

$$f(\xi, D) = \sum_{i=0}^{\infty} \alpha_i(D)\Psi_i(\xi) \tag{10}$$

where α are the coefficients representing the deterministic component and Ψ are the basis functions representing the stochastic component, such that the basis functions are orthonormal with respect to the probability distribution of ξ, $\pi(\xi)$.

$$\int \Psi_i(\xi)\Psi_j(\xi)\pi(\xi)d\xi = \delta_{i,j} \tag{11}$$

All variables in this work were assumed to be normally distributed, as stated by the central limit theorem. Therefore, the corresponding basis functions Ψ for such a distribution are the Hermite polynomials [48]. Here, the n-D basis functions Ψ are defined as a tensor product of one-dimensional basis functions ϕ.

To guarantee convergence in the expansion, the series given in Eq. (10) should be infinite ($P = \infty$). The series is however truncated at some finite number to be computationally feasible. For a polynomial order n and the number of random variables s, the series truncation scheme is defined by Xiu and Karniadakis [48]

$$N_t = P + 1 = \frac{(n+s)!}{n!s!} \tag{12}$$

where N_t is the total number of terms and s is the number of random variables. A polynomial of second-order ($n = 2$) is used throughout this work. Reddy [49] showed that a second order polynomial approximation was sufficient to accurately recover the probability distribution obtained using Monte Carlo sampling with a large number of samples.

The PCE framework present can be used in an intrusive or a nonintrusive fashion. The intrusive PCE approach requires modification to the numerical solver by incorporating the PCE in Eq. (10) directly into the governing equations or discretized equations. This has shown to be computationally expensive [44].

The nonintrusive PCE approach constructs a surrogate model by fitting the PCE expansion in Eq. (10) to a sequence of generated samples. A total of N_t samples are generated by obtaining the response of the system at various randomly generated values of input parameters. These random values of the variables are drawn from the probability distribution of those variables. A linear system of size N_t can be formulated, Eq. (13), and solved to obtain the coefficients of the deterministic component. It should be noted that if exactly N_t samples are available, then the surrogate construction becomes an interpolation problem. If the number of samples is greater than N_t then the least-squares approach is needed to

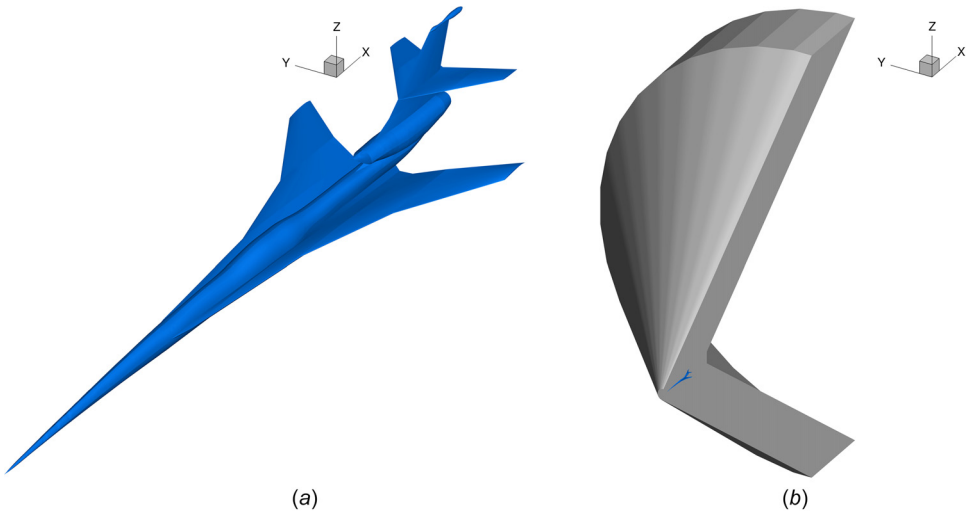

(*a*) (*b*)

Fig. 1 (*a*) Rendering of the NASA Concept 25D low-boom supersonic aircraft and (*b*) Symmetric computational mesh domain for supersonic CFD simulations [57]

solve the system of equation. The number of samples over the required minimum, N_t, is represented by the oversampling ratio (OSR). Hosder et al. [50] determined that an optimal value of OSR is 2.0. Therefore, twice the number of minimum required samples were generated in each uncertainty quantification (UQ) study, and the system was solved using a least-squares approach.

$$\begin{pmatrix} \Psi_0(\xi_0) & \Psi_1(\xi_0) & \cdots & \Psi_p(\xi_0) \\ \Psi_0(\xi_1) & \Psi_1(\xi_1) & \cdots & \Psi_p(\xi_1) \\ \vdots & \vdots & \ddots & \vdots \\ \Psi_0(\xi_P) & \Psi_1(\xi_P) & \cdots & \Psi_p(\xi_P) \end{pmatrix} \begin{pmatrix} \alpha_0 \\ \alpha_1 \\ \vdots \\ \alpha_P \end{pmatrix} = \begin{pmatrix} f(\xi_0, D) \\ f(\xi_1, D) \\ \vdots \\ f(\xi_P, D) \end{pmatrix} \tag{13}$$

Once the system in Eq. (13) is solved, the mean and variance can be obtained using Eqs. (14) and (15), respectively. The uncertainty quantification using PCE was done using the Chaospy toolbox [51].

$$\mu_f = \langle f \rangle \approx \sum_{i=0}^{P} \alpha_i(D) \langle \Psi_i(\xi) \rangle = \alpha_0 \tag{14}$$

$$\sigma_f^2 = \langle (f - \mu_f)^2 \rangle \approx \left\langle \left(\sum_{i=0}^{P} \alpha_i(D) \Psi_i(\xi) \right)^2 \right\rangle = \sum_{i=1}^{P} \alpha_i^2(D) \langle \Psi_i^2(\xi) \rangle \tag{15}$$

The global sensitivity of the response to variables can also be represented by computing the Sobol's indices. Once the PCE coefficients are computed, they can be used to analytically compute the Sobol's indices [52,53], from this equation

$$\mathcal{S}_u = \frac{\sum_{k \in K_u} \alpha_k^2 \langle \Psi_k, \Psi_k \rangle}{\sum_{k=0}^{P} \alpha_k^2 \langle \Psi_k, \Psi_k \rangle} \tag{16}$$

where

$$K_u = \{k \in \{1, \ldots, P\} | \Psi_k(\xi) = \prod_{i=1}^{|u|} \phi_{\alpha_i^k}(\xi_{u_i}), \alpha_i^k > 0\} \tag{17}$$

The total Sobol's indices can then be computed as

$$\mathcal{S}_{T_i} \equiv \sum_{u \ni i} \mathcal{S}_u \tag{18}$$

3 Computational Fluid Dynamics Analysis of C25D Aircraft

The sonic boom pressure signature was obtained by solving the Euler equations around the aircraft geometry using UNS3D. The aircraft geometry in this work was the NASA Concept 25D (C25D), Fig. 1(*a*). This aircraft was designed to achieve an undertrack sonic boom loudness of 74.2 PLdB [54], and the design was further refined to reduce the sonic boom signature of the entire boom carpet [55]. The C25D configuration features a reference length of 32.92 m and a reference half-span area of 37.16 m^2. The aircraft was assumed to be traveling at a Mach number of 1.6 at an altitude of 15.76 km [56] under standard atmospheric conditions. The computational mesh was taken from the Second AIAA Sonic Boom Prediction Workshop (SBPW2) [56]. The mesh contained 3,419,776 nodes defining 5,564,030 tetrahedral and 4,810,500 prism elements. The computation domain is shown in Fig. 1(*b*).

Figure 2(*a*) shows the convergence history of the field variables. A steady, stable convergence in the residual is seen. The convergence of the integrated forces and moments was also found to be well-behaved. The convergence history for the lift-to-drag ratio (L/D) in Fig. 2(*b*) shows that a converged value for the integrated forces was reached after only 200 iterations.

Table 1 shows the aerodynamic coefficient of lift c_l, coefficient of drag $c_{d,}$ and coefficient of moment c_m computed using UNS3D and the mean and standard deviation of the coefficients computed in the SBPW2. It can be seen that PLdB computed using near-field signature calculated by UNS3D is in good agreement (within 1% relative error) to that obtained in the SBPW2.

Figure 3(*a*) shows the location of the pressure extraction sensor relative to the aircraft geometry. Figure 3(*b*) shows the near-field pressure (red dashed-line), extracted along the undertrack of the aircraft at a distance R of five body lengths L, plotted against the mean workshop data (black dotted-line) from the SBPW2 obtained using various Euler-based CFD computations. It should be mentioned that the near-field pressure is computed as $\Delta p/p_\infty$, where p_∞ is the freestream pressure and $\Delta p = p - p_\infty$. It was found that the current prediction matched well with the workshop data, roughly falling within a standard deviation of the ensemble data. This pressure signature was then propagated using sBOOM

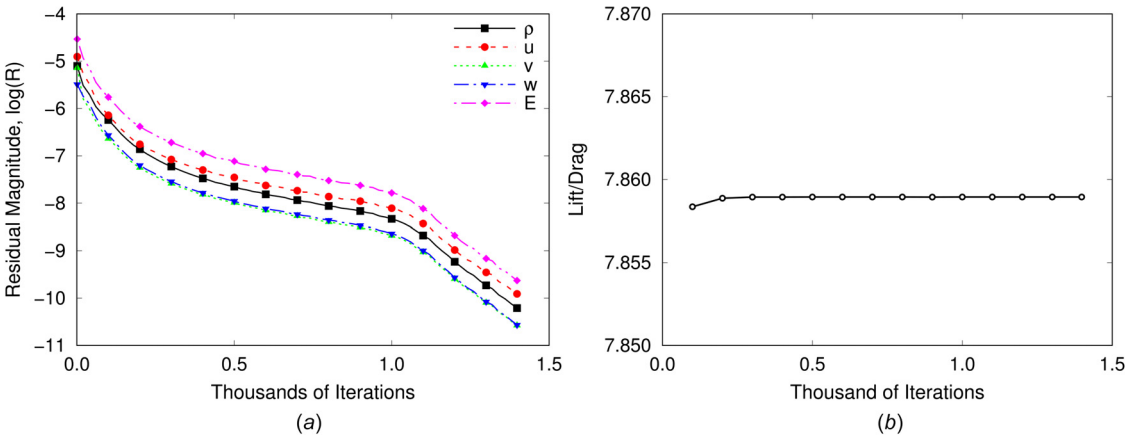

Fig. 2 Convergence histories for the baseline aircraft simulation showing: (*a*) residual of field variables and (*b*) lift-to-drag coefficient

Table 1 Comparison of predicted aerodynamic coefficients and undertrack PLdB with SBPW2 data

	c_l	c_d	c_m	PLdB
UNS3D	0.0687	0.00874	−0.0523	80.86
SBPW2 ($\mu \pm \sigma$)	0.0680 ± 0.0001	0.00900 ± 0.00001	-0.0518 ± 0.0001	80.23 ± 0.57
UNS3D/SBPW2-1	1.04%	−2.88%	0.95%	0.78%

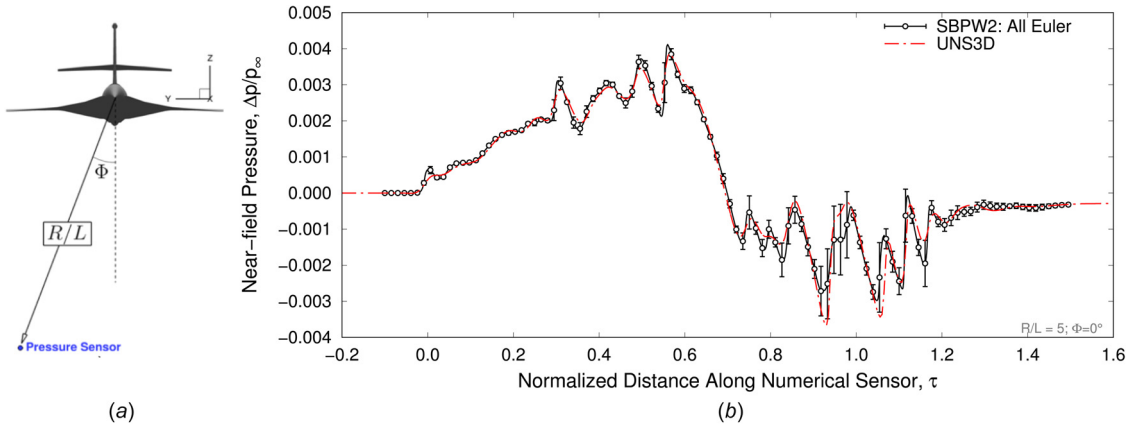

Fig. 3 (*a*) Sensor location from a head-on view and (*b*) comparison of the current near-field pressure signature compared against the mean and standard deviation of all Euler solutions submitted to SBPW2

and was used for all sensitivity analysis and uncertainty quantification studies.

4 Sensitivity Analysis

4.1 Sensitivity of Perceived Level to Altitude. A preliminary sensitivity analysis was performed to identify the altitude range that contribute most to the change in sonic boom loudness. This can be done using the sensitivity coefficients of the PL. The sensitivity of Y to changes in parameter T can be defined using the sensitivity coefficient, Σ given by

$$\Sigma_T(Y) = \frac{\partial Y}{\partial T} \tag{19}$$

Using this definition of sensitivity coefficients, the sensitivity of PL due to each atmospheric variable at various altitudes is obtained. The sensitivity study is performed about the mean of

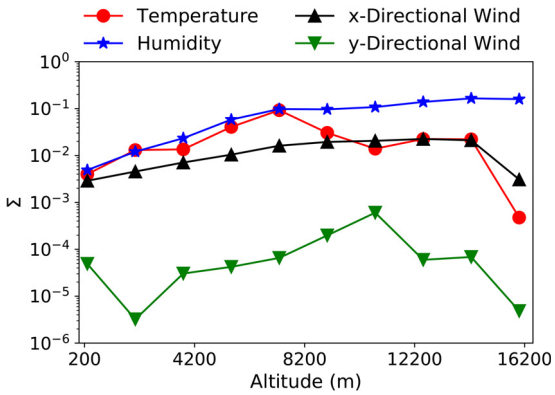

Fig. 4 Sensitivity of coefficient of sonic boom loudness at various altitudes with respect to temperature, relative humidity, x-directional winds, and y-directional winds

variables of the combined set containing profiles for all six cities. Figure 4 shows the sensitivity coefficients of ground PL to various altitudes due to each of the four atmospheric variables. It is immediately evident that the overall loudness is not sensitive to any particular altitude. It can be seen that the loudness metrics are least sensitive to the y-directional winds for an aircraft heading in the positive x direction. Figure 4 shows that the boom propagation might be more sensitive to the complete atmospheric profile than to any particular range of the profile. This assumption is further validated by performing the uncertainty quantification studies. Since the y-directional wind does not contribute much to the sonic boom loudness, it was removed from the set of variables in the UQ study presented in Sec. 5.

4.2 Sensitivity Analysis of Perceived Level Due to Atmospheric Variables. The atmospheric profiles for the year 2017 for six cities around the world is used for sensitivity analysis. The cities, namely, Miami, Mumbai, Oslo, Glasgow, Shanghai, and Las Vegas are well diversified in terms of their geographical location and weather conditions year-round. The distributions for temperature, humidity, x and y directional wind for all the six cities can be found in the Appendix. The variables that affect propagation of the sonic boom and its PL, such as relative humidity, temperature, x-directional wind velocity, and y-directional wind velocity are chosen as input parameters for the sensitivity analysis. The pressure profile was again obtained by imposing the hydrostatic balance. The raw data captured values of all the input

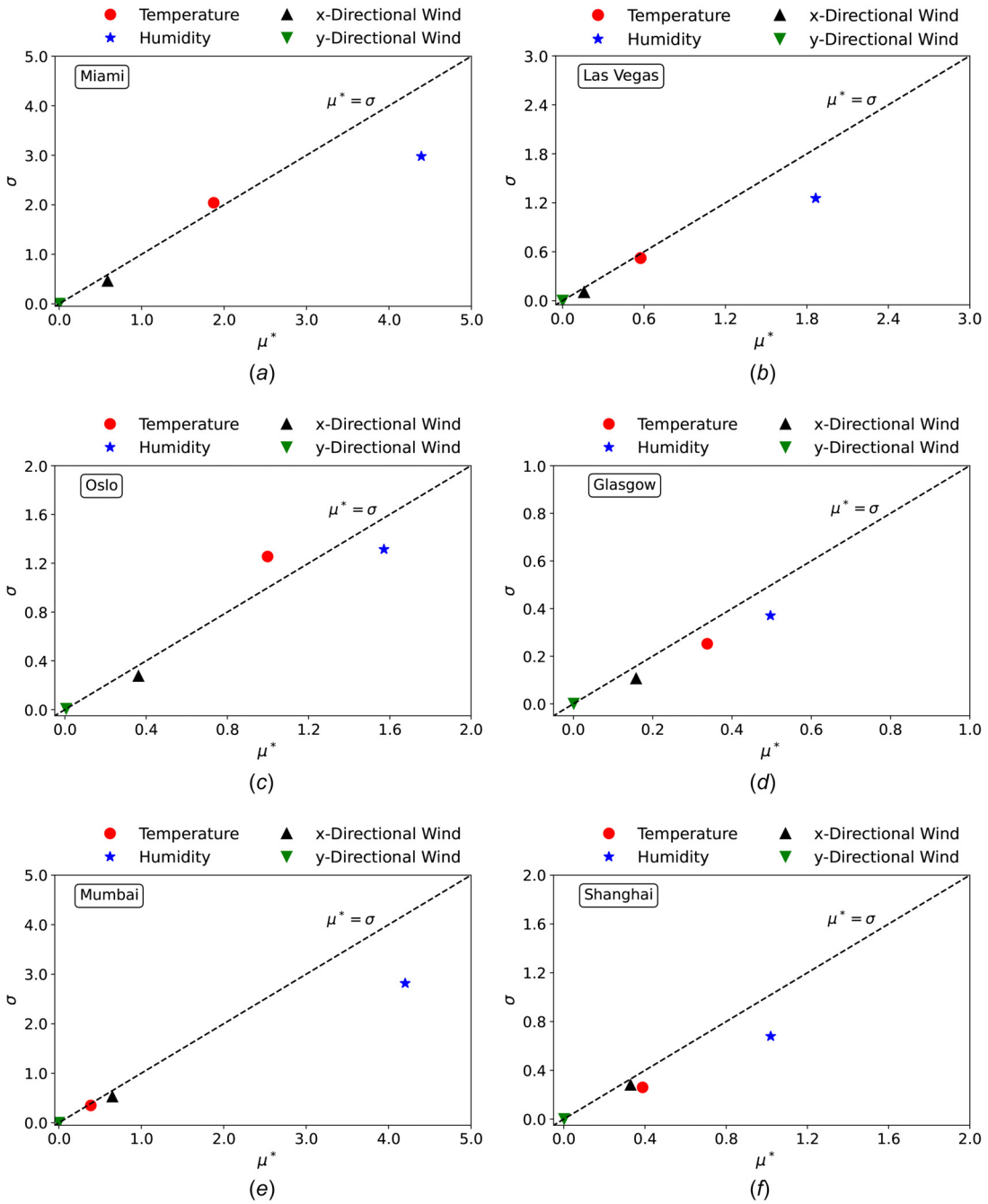

Fig. 5 The mean and standard deviation of the elementary effects of the four variables for: (*a*) Miami, (*b*) Las Vegas, (*c*) Oslo, (*d*) Glasgow, (*e*) Mumbai, and (*f*) Shanghai

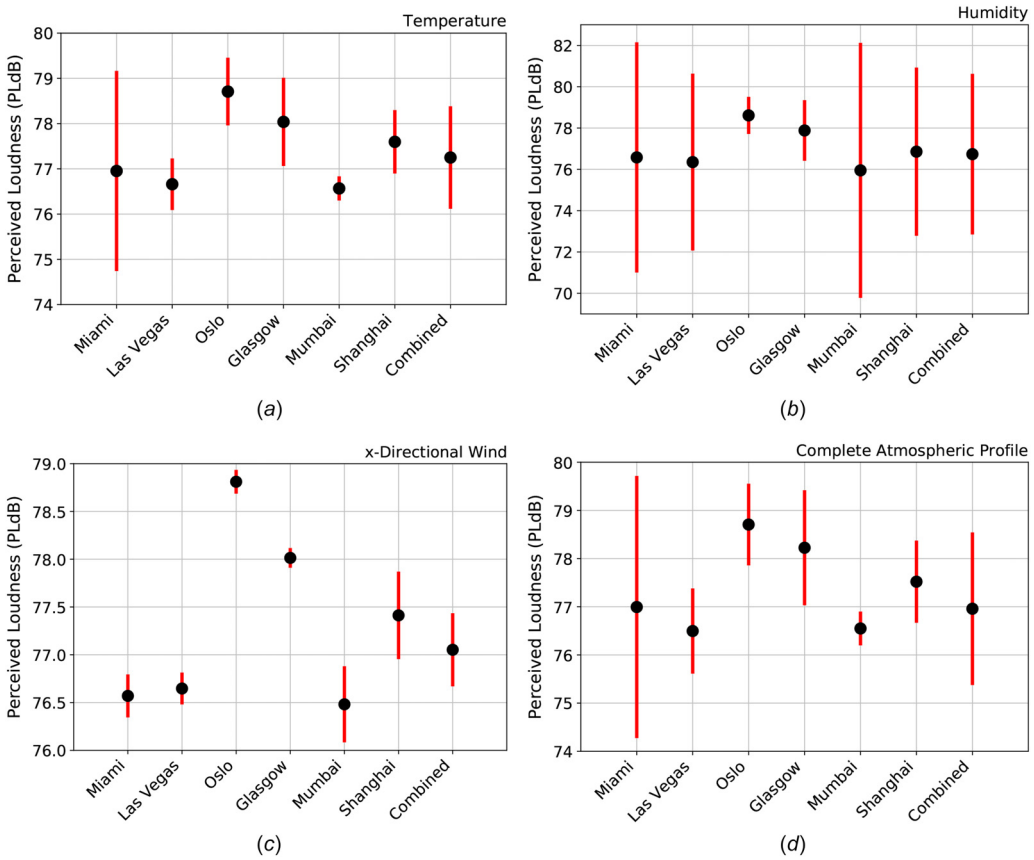

Fig. 6 Mean (black) and standard deviation (red) of the PL at each of the six cities and combined set of cities due to: (*a*) temperature profile, (*b*) humidity profile, (*c*) x-directional winds, and (*d*) complete atmospheric profile

Table 2 Mean and standard deviation (in brackets) of sonic boom loudness due to uncertainty in all atmospheric variables

Variable	Miami	Las Vegas	Oslo	Glasgow	Mumbai	Shanghai	Combined
Temperature	77.0 (2.2)	76.7 (0.5)	78.7 (0.7)	78.0 (0.9)	76.6 (0.2)	77.6 (0.7)	77.3 (1.1)
Humidity	76.6 (5.5)	76.4 (4.2)	78.6 (0.8)	77.9 (1.4)	76.0 (6.1)	76.9 (4.0)	76.7 (3.8)
x-Directional winds	76.6 (0.2)	76.6 (0.1)	78.8 (0.1)	78.0 (0.1)	76.5 (0.4)	77.4 (0.4)	77.1 (0.4)
Complete profile	77.0 (2.7)	76.5 (0.8)	78.7 (0.8)	78.2 (1.2)	76.5 (0.3)	77.5 (0.8)	77.0 (1.5)

variables at ten different altitudes uniformly spaced from 200 to 16,200 m, noting that 16,200 m is above the C25D's cruising altitude. The raw data contained different number of profiles at each day of the year. Monthly averages were calculated for all four variables at each altitude. Atmospheric profiles from IGRA are typically available at 0:00 and 12:00 UTC, however data was occasionally missing or available at other times and months. One profile was defined for each city for each month. The profile for a given variable is comprised of one monthly average value for each altitude. Twelve unique profiles each for Mumbai, Shanghai, Glasgow, and Las Vegas, eleven unique profiles for Oslo and ten unique profiles for Miami were defined for each variable.

Unique combinations or samples are generated using ReSU sampling strategy. Nominal distribution with number of categories equal to number of months were assigned to all the variables. The number of trajectories selected to generate a sample for Mumbai, Shanghai, Glasgow, and Las Vegas are 66, for Oslo are 55 and for Miami are 45. The number of samples generated for Mumbai, Shanghai, Glasgow, and Las Vegas are 330, for Oslo are 275 and for Miami are 225. A total of 1820 runs of the sBOOM model were conducted. The value of the PL was recorded for each of the samples, and sensitivity measures are calculated based on them. Categorization of input parameters into important and unimportant model parameters is achieved through plotting μ^* versus σ.

The absolute mean and standard deviation of the elementary effects for each city are presented in Fig. 5. In the μ^* versus σ space, y-directional wind is very close to the origin for all six cities indicating that it is an unimportant parameter and has little effect on the loudness. The magnitude of the y component of wind speed is typically lower than the x component and, therefore, it has minimal impact on the model output in part, due to the choice of the aircraft's heading for this analysis. Relative humidity is well-separated from the $\mu^* = \sigma$ line and farthest from the origin, identifying it as the most important model parameter to affect the PL for all six cities. Temperature is the second model parameter well-separated from the origin in all cities except Mumbai and Shanghai. Hence, temperature can be attributed the status of second most important model parameter. x-directional wind is the third model parameter in terms of separation from the origin at Miami, Glasgow, Oslo, and Las Vegas. In the case of Mumbai

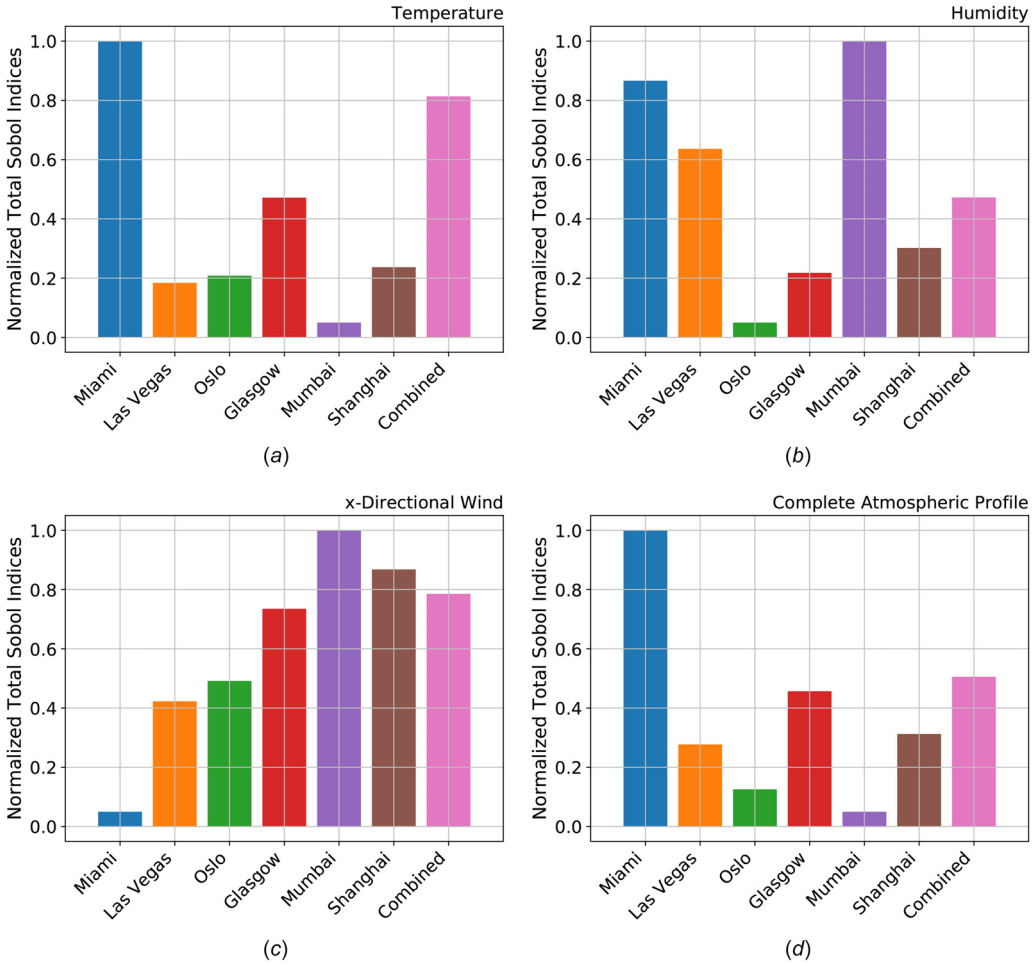

Fig. 7 Normalized total Sobol's indices at each of the six cities and combined set of cities due to: (*a*) temperature profile, (*b*) humidity profile, (*c*) x-directional winds, and (*d*) complete atmospheric profile

and Shanghai, the sensitivity of PL on temperature is nearly equivalent to that of the x-directional wind. Also, both temperature and x-directional wind velocity are very close to the $\mu^* = \sigma$ line indicating they have both linear impact as well as interactions effect for Mumbai and Shanghai.

5 Uncertainty Quantification of Perceived Level Due to Atmospheric Profile

An uncertainty quantification study was performed to identify the effects of atmospheric profiles on sonic boom loudness. The UQ was performed using data for each of the six cities and using the data of the combined set of the six cities. The distribution of each variable at each city is given in Appendix. The profile defined its value at ten different altitudes, uniformly distributed from 200 to 16,200 m. Therefore, $s = 10$ in Eq. (12) for each uncertainty quantification study, since the value of the parameter at each of the ten altitudes is considered an uncertain parameter. It should be mentioned that only the uncertain variables are sampled from their probability distribution, while the remaining variables are constrained to their mean values. For example, UQ of loudness due to temperature profile only deals with sampling the temperature profile from its given distribution and constraining the humidity and wind profiles to their mean values.

The uncertainty in sonic boom loudness due to uncertainty in temperature profile is calculated using the nonintrusive PCE approach. Figure 6(*a*) shows the mean and the standard deviation in loudness for each of the seven data sets. The uncertainty in loudness is not consistent in each of the seven data sets. Figure 6(*a*) and Table 2 show that there is greater uncertainty due to temperature in Miami followed by Glasgow. Loudness values in Las Vegas and Mumbai are least affected by uncertainty in temperature since the temperature profiles at these locations have little variation throughout the year. The difference between the maximum loudness (Oslo) and minimum loudness (Mumbai) is approximately 2.1 PLdB. This suggests that different atmospheric variables influence the loudness more, depending on the profile of the remaining atmospheric variables. This is investigated by computing the influence of the remaining atmospheric variables.

The uncertainty in sonic boom loudness due to uncertainty in relative humidity profile is calculated. Figure 6(*b*) shows the mean and the standard deviation in loudness at each of the seven data sets. Comparing Figs. 6(*a*) and 6(*b*) shows that the pattern for mean loudness is similar in both cases. Oslo remains the city with the highest PL and Mumbai remains the lowest. The difference between maximum loudness and minimum loudness is approximately 2.6 PLdB. Figure 6(*b*) and Table 2 show that the uncertainty in PL is greatly influenced by the uncertainty in relative humidity. It is evident in the higher standard deviation values as compared to those due to temperature. It shows that humidity has greater influence than temperature on the PL. Both loudness values in Oslo and Glasgow are least affected by the humidity. This is mainly due to the small variation in their humidity profiles throughout the year as shown in the Appendix.

The uncertainty in sonic boom loudness due to uncertainty in x-directional wind profile is calculated. Figure 6(*c*) shows the mean and the standard deviation in loudness at each of the seven data sets. It can be seen that the mean loudness for each of the seven data sets in Fig. 6(*c*) is similar to that of Fig. 6(*a*) and also follows similar patterns as Fig. 6(*b*). Since mean loudness in Fig. 6(*c*) are similar to those in Fig. 6(*a*), it indicates that the large differences between Figs. 6(*b*) and 6(*c*) are primarily due to the uncertainty in humidity. Oslo again experiences a higher PL and Mumbai the lowest PL with a difference of 2.3 PLdB between them. The relatively small standard deviations in PL indicate the small influence of uncertainty in x-directional winds on the loudness, despite each of the seven data sets having a large variation in x-directional wind profile. It should however be mentioned that in certain cities (Mumbai and Shanghai), the effects of x-directional winds are equally as important as temperature.

Thus far, the uncertainties in a profile of a single variable at a time are considered to identify the variables that most influence the PL. Here, the uncertainty quantification is performed using all three variable profiles for each of the seven data sets. In this study, the total number of uncertain parameters is $s = 30$; 10 altitudes for each of the three variables. Figure 6(*d*) shows that mean and standard deviation of PL for each of the seven data sets. The mean values continue to follow similar trend as before. It shows the large changes in PL that are possible as an aircraft flies from one location to another. Mumbai experiences a lower variability in boom loudness.

Figure 7(*d*) shows the total Sobol's indices normalized between 0.1 and 1.0. It can be seen that the temperature profile has a significant effect on the PL in Miami. The x-directional wind and humidity profiles greatly influence the PL in Mumbai. Similar trends were seen in Fig. 6.

6 Conclusion

The effects of uncertainty in atmospheric profile on perceived sonic boom loudness are examined. Sensitivity analysis was also performed to investigate the effects of altitude range and atmospheric variables on sonic boom loudness. The uncertainties in atmospheric profiles of temperature, relative humidity, and wind are propagated through the sonic boom propagation software sBOOM using nonintrusive polynomial chaos. It was shown that sonic boom loudness is most influenced by the humidity profile followed by the temperature and x-directional wind profiles. Sensitivity analysis showed that y-directional winds do not contribute much to the ground loudness. It also showed that there is no particular altitude range that significantly contributes to the overall loudness. This study shows that the wind profiles can be neglected, in some but not all cities, during low-boom aircraft optimization under atmospheric uncertainty without significantly compromising the accuracy.

Acknowledgment

The lead author gratefully acknowledges the financial support from Florida International University in the form of an FIU Presidential Fellowship and FIU Dissertation Year Fellowship. This work is supported by the NASA HQ University Leadership Initiative (ULI) Program under federal award number NNX17AJ96A, titled "Adaptive Aerostructures for Revolutionary Supersonic Transportation" managed by Texas A & M University. Authors are deeply indebted to Professor Paul Cizmas from Texas A & M University for using results from his UNS3D code and to Professor Doug Hunsaker from Utah State University for using his PyLdB code. We also thank the two anonymous reviewers for their thorough reviews and useful suggestions, which helped improve the conclusions and clarity of the paper.

Appendix

This section shows the atmospheric profiles for each of the four atmospheric variables in each of the six cities (Figs. 8–11).

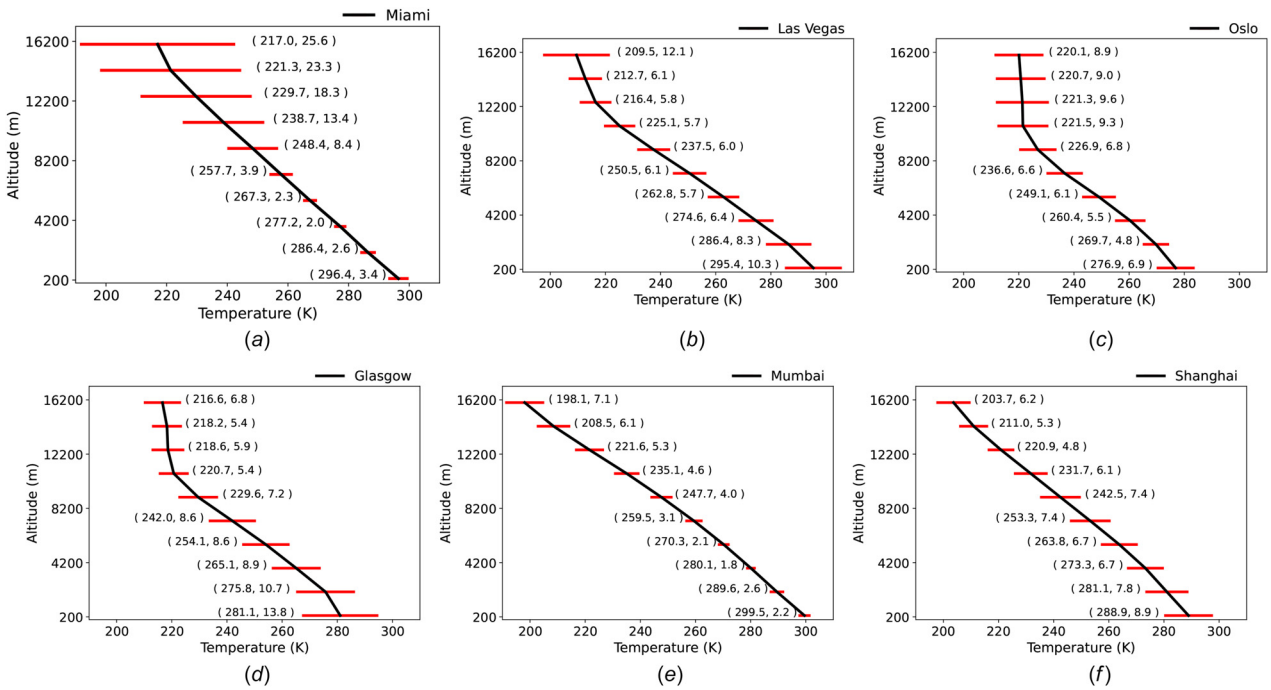

Fig. 8 Mean (black) and standard deviation (red) of temperature profiles for: (*a*) Miami, (*b*) Las Vegas, (*c*) Oslo, (*d*) Glasgow, (*e*) Mumbai, and (*f*) Shanghai. The mean μ and standard deviation σ is given in the parenthesis as (μ, σ).

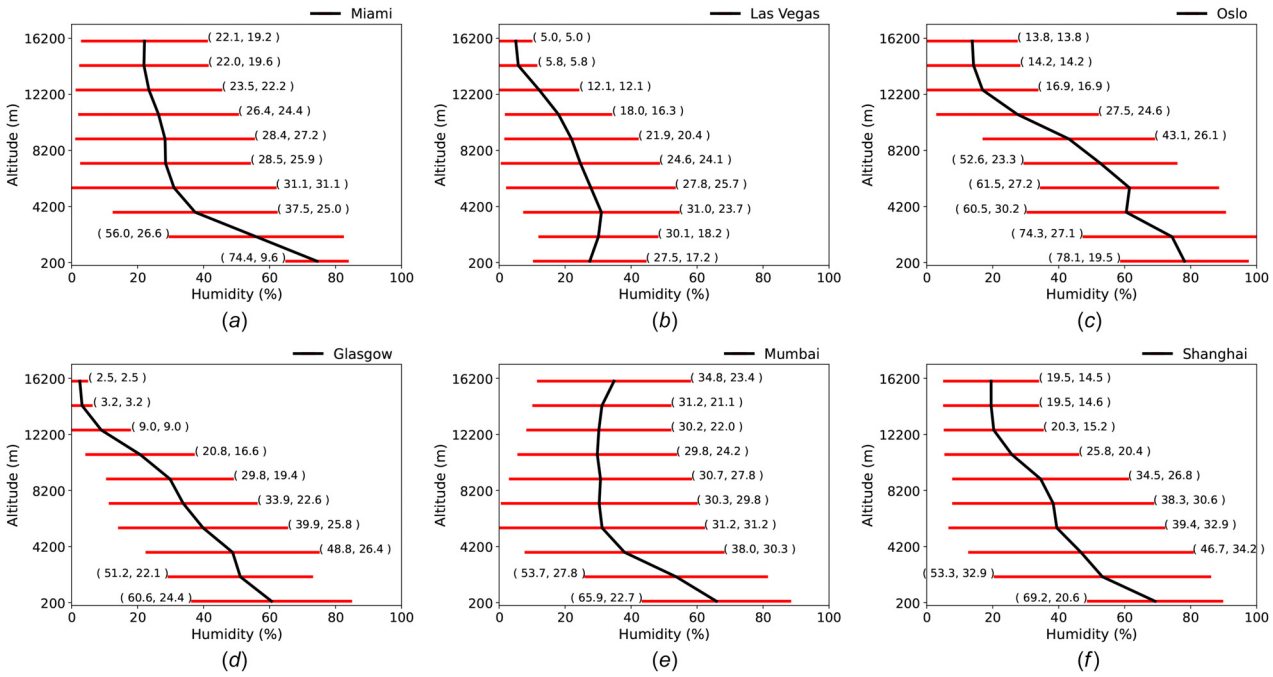

Fig. 9 Mean (black) and standard deviation (red) of relative humidity profiles for: (*a*) Miami, (*b*) Las Vegas, (*c*) Oslo, (*d*) Glasgow, (*e*) Mumbai, and (*f*) Shanghai. The mean μ and standard deviation σ is given in the parenthesis as (μ, σ).

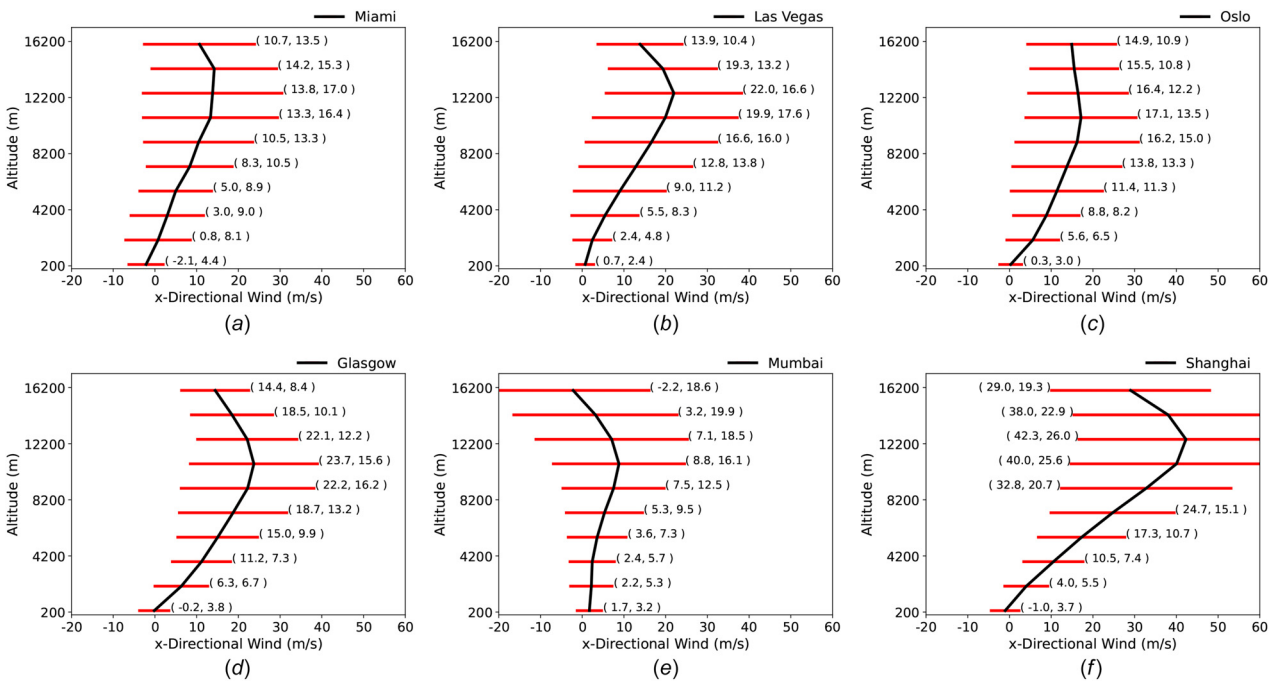

Fig. 10 Mean (black) and standard deviation (red) of x-directional wind profiles for: (*a*) Miami, (*b*) Las Vegas, (*c*) Oslo, (*d*) Glasgow, (*e*) Mumbai, and (*f*) Shanghai. The mean μ and standard deviation σ is given in the parenthesis as (μ, σ).

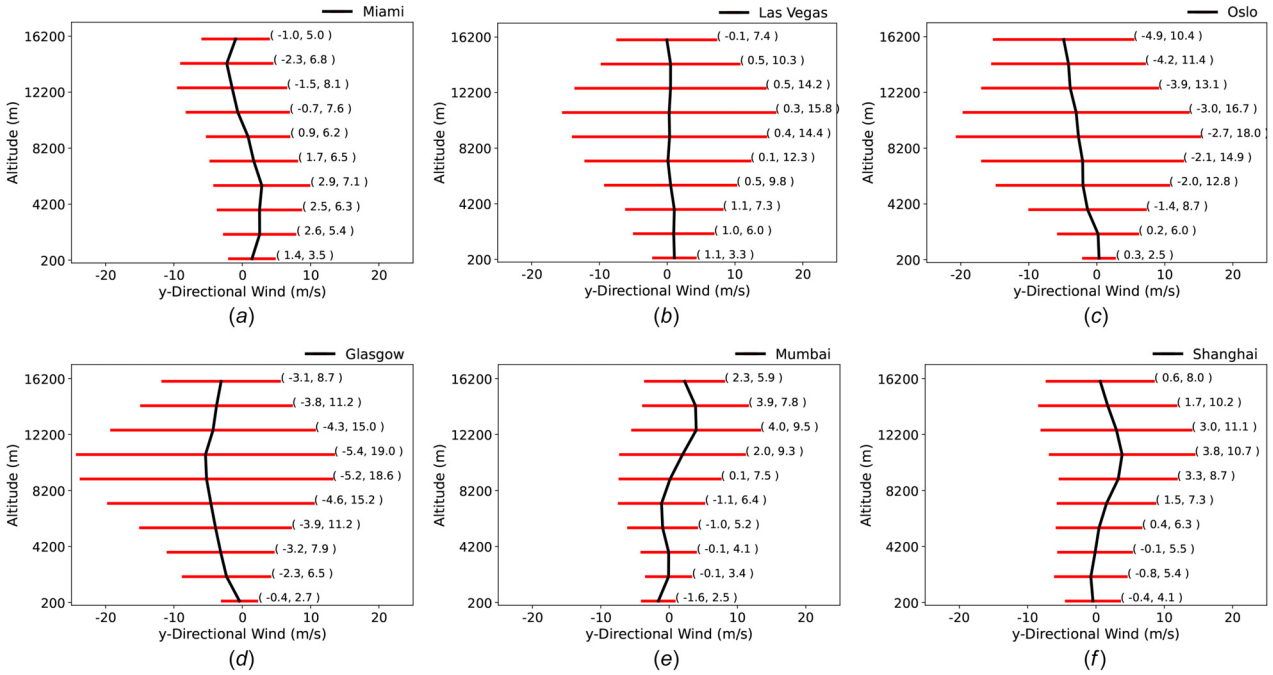

Fig. 11 Mean (black) and standard deviation (red) of y-directional wind profiles for: (*a*) Miami, (*b*) Las Vegas, (*c*) Oslo, (*d*) Glasgow, (*e*) Mumbai, and (*f*) Shanghai. The mean μ and standard deviation σ is given in the parenthesis as (μ, σ).

References

[1] Prather, M. J., Wesoky, H. L., Miake-Lye, R. C., Douglass, A. R., Turco, R. P., Wuebbles, D. J., Ko, M., and Schmeltekopf, A. L., 1992, "The Atmospheric Effects of Stratospheric Aircraft: A First Program Report," National Aeronautics and Space Administration, Washington, DC, Report No. RP-1272.

[2] Pawlowski, J., Graham, D., Boccadoro, C., Coen, P., and Maglieri, D., 2005, "Origins and Overview of the Shape Sonic Boom Demonstration Program," AIAA Paper No. 2005-5.

[3] Aftosmis, M., Nemec, M., and Cliff, S., 2011, "Adjoint-Based Low-Boom Design With Cart3D," AIAA Paper No. 2011–3500.

[4] Howe, D., Simmons, F., and Freund, D., 2008, "Development of the Gulfstream Quiet Spike (TM) for Sonic Boom Minimization," AIAA Paper No. 2008–124.

[5] Xiaoqiang, F., Zhanke, L., and Bifeng, S., 2014, "Research of Low Boom and Low Drag Supersonic Aircraft Design," Chin. J. Aeronaut., **27**(3), pp. 531–541.

[6] Chan, M. K., 2003, "Supersonic Aircraft Optimization for Minimizing Drag and Sonic Boom," Ph.D. thesis, Stanford University, Stanford, CA.

[7] Reddy, S. R., Dulikravich, G. S., Carpenter, F. L., and Cizmas, P. G., 2019, "Achieving Quieter Supersonic Flight Through Outer-Mold Line Modifications: An Optimization Study," AIAA Paper No. 2019-3104.

[8] Rallabhandi, S. K., West, T. K., and Nielsen, E. J., 2017, "Uncertainty Analysis and Robust Design of Low-Boom Concepts Using Atmospheric Adjoints," AIAA J. Aircr., **54**(3), pp. 902–917.

[9] West, T., Reuter, B., Walker, E., Kleb, W. L., and Park, M. A., 2017, "Uncertainty Quantification and Certification Prediction of Low-Boom Supersonic Aircraft Configurations," AIAA J. Aircr., **54**(1), pp. 40–53.

[10] Fujino, K., Kikuchi, R., Shimoyama, K., Obayashi, S., and Makino, Y., 2017, "Effects of Uncertainties in Atmospheric Turbulence and Weather Predictions on Sonic Boom," AIAA Paper No. 2017–0280.

[11] Shimoyama, K., Ono, D., Hashimoto, A., Jeong, S., and Obayashi, S., "2012, "Sonic Boom Analysis Under Atmospheric Uncertainties by a Non-Intrusive Polynomial Chaos Method," 10th World Congress on Computational Mechanics, Sao Paulo, Brazil, July 8–13, pp. 342–350.

[12] Jeong, S., Ono, D., Shimoyama, K., and Hashimoto, A., 2013, "Sonic Boom Analysis Under Conditions of Atmospheric Uncertainty Using Polynomial Chaos," Trans. Jpn. Soc. Aeronaut. Space Sci., **56**(3), pp. 129–136.

[13] Stevens, S., 1972, "Perceived Level of Noise by Mark VII and Decibels (E)," J. Acoust. Soc. Am., **51**(2B), pp. 575–601.

[14] DeGolia, J., and Loubeau, A., 2017, "A Multiple-Criteria Decision Analysis to Evaluate Sonic Boom Noise Metrics," J. Acoust. Soc. Am., **141**(5), pp. 3624–3624.

[15] Loubeau, A., Wilson, S. R., and Rathsam, J., 2018, "Updated Evaluation of Sonic Boom Noise Metrics," J. Acoust. Soc. Am., **144**(3), pp. 1706–1706.

[16] Rallabhandi, S. K., 2011, "Advanced Sonic Boom Prediction Using the Augmented Burgers Equations," AIAA J. Aircr., **48**(4), pp. 1245–1253.

[17] Han, Z.-X., and Cizmas, P. G., 2003, "A CFD Method for Axial Thrust Load Prediction of Centrifugal Compressors," Int. J. Turbo Jet-Engines, **20**(1), pp. 1–16.

[18] Roe, P. L., 1981, "Approximate Riemann Solvers, Parameter Vectors, and Difference Schemes," J. Comput. Phys., **43**(2), pp. 357–372.

[19] Harten, A., and Hyman, J. M., 1983, "Self -Adjusting Grid Methods for One-Dimensional Hyperbolic Conservation Laws," J. Comput. Phys., **50**(2), pp. 235–269.

[20] Barth, T., 1991, "A 3D Upwind Euler Solver for Unstructured Meshes," AIAA Paper No. 91-1548.

[21] Saad, Y., and Schultz, M. H., 1986, "GMRES: A Generalized Minimal Residual Algorithm for Solving Nonsymmetric Linear Systems," SIAM J. Sci. Stat. Comput., **7**(3), pp. 856–869.

[22] National Oceanic and Atmospheric Administration National Centers for Environmental Information, 2018, "Integrated Global Radiosonde Archive," National Oceanic and Atmospheric Administration National Centers for Environmental Information, Asheville, NC, Mar. 12, 2020, https://www.ncdc.noaa.gov/data-access/weather-balloon/integrated-global-radiosonde-archive

[23] Durre, I., Vose, R., and Wuertz, D., 2006, "Overview of the Integrated Global Radiosonde Archive," J. Clim., **19**(1), pp. 53–68.

[24] Pierce, A. D., 1989, *Acoustics an Introduction to Its Physical Principles and Applications*, Acoustical Society of America, New York.

[25] Sullivan, B., 2004, "Human Response to Simulated Low Intensity Sonic Boom," Proceedings of NOISE-CON 2004, pp. 541–550.

[26] Pyldb, 2019, "PyLdB," accessed Mar. 21, 2020, https://github.com/usuaero/PyLdB

[27] Park, M., 2016, "2nd AIAA Sonic Boom Prediction Workshop: C25D Flow Through Nacelle," accessed Nov. 2019, https://lbpw.larc.nasa.gov/sbpw2/near-field/c25d-flowthru/

[28] Landau, L., and Lifshitz, E., 1959, *Fluid Mechanics: Volume 6 of Course of Theoretical Physics*, Pergamon Press, Oxford, UK.

[29] Gad-el-Hak, M., 1995, "Stokes' Hypothesis for a Newtonian, Isotropic Fluid," ASME J. Fluids Eng., **117**(1), pp. 3–5.

[30] Dulikravich, G. S., 2001, "Stokes' Hypothesis and Entropy Variation Within a Compression Shock," 23rd International Symposium on Shock Waves, Fort Worth, TX, July 22–27, pp. 1–7.

[31] Dulikravich, G. S., and Kennon, S. R., 1988, "Theory of Compressible Irrotational Flows Including Heat Conductivity and Longitudinal Viscosity," Int. J. Math. Comput. Modell., **10**(8), pp. 583–592.

[32] Truesdell, C., 1954, "The Present Status of the Controversy Regarding the Bulk Viscosity of Fluids," Proc. R. Soc. London, Ser. A: Math. Phys. Sci., **226**(5), pp. 59–65.

[33] Morris, M. D., 1991, "Factorial Sampling Plans for Preliminary Computational Experiments," Technometrics, **33**(2), pp. 161–174.

[34] Khare, Y., Martinez, C. J., Muñoz-Carpena, R., Bottcher, A. D., and James, A., 2019, "Effective Global Sensitivity Analysis for High-Dimensional Hydrologic and Water Quality Models," J. Hydrologic Eng., **24**(1), p. 04018057.

[35] Campolongo, F., Saltelli, A., and Cariboni, J., 2011, "From Screening to Quantitative Sensitivity Analysis. A Unified Approach," Comput. Phys. Commun., **182**(4), pp. 978–988.

[36] Sohier, H., Piet-Lahanier, H., and Farges, J.-L., 2015, "Analysis and Optimization of an Air-Launch-to-Orbit Separation," Acta Astronaut., **108**, pp. 18–29.

[37] Yuan, Y., Khare, Y., Wang, X., Parajuli, P. B., Kisekka, I., and Finsterle, S., 2015, "Hydrologic and Water Quality Models: Sensitivity," Trans. ASABE, **58**(6), pp. 1721–1744.

[38] Sanchez, D. G., Lacarrière, B., Musy, M., and Bourges, B., 2014, "Application of Sensitivity Analysis in Building Energy Simulations: Combining First- and Second-Order Elementary Effects Methods," Energy Build., **68**, pp. 741–750.
[39] Fezi, K., and Krane, M. J. M., 2017, "Uncertainty Quantification in Modelling Equiaxed Alloy Solidification," Int. J. Cast Met. Res., **30**(1), pp. 34–49.
[40] Campolongo, F., Cariboni, J., and Saltelli, A., 2007, "An Effective Screening Design for Sensitivity Analysis of Large Models," Environ. Modell. Software, **22**(10), pp. 1509–1518.
[41] Khare, Y., Munoz-Carpena, R., Rooney, R., and Martinez, C. J., 2015, "A Multi-Criteria Trajectory-Based Parameter Sampling Strategy for the Screening Method of Elementary Effects," Environ. Modell. Software, **64**, pp. 230–239.
[42] Chitale, J., Khare, Y., Muoz-Carpena, R., Dulikravich, G. S., and Martinez, C., 2017, "An Effective Parameter Screening Strategy for High Dimensional Models," ASME Paper No. IMECE2017-71458.
[43] Xiao, S., Lu, Z., and Xu, L., 2016, "A New Effective Screening Design for Structural Sensitivity Analysis of Failure Probability With the Epistemic Uncertainty," Reliab. Eng. Syst. Saf., **156**, pp. 1–14.
[44] Hosder, S., and Bettis, B., 2012, "Uncertainty and Sensitivity Analysis for Reentry Flow With Inherent and Model- Form Uncertainties," J. Spacecr. Rockets, **49**(2), pp. 193–206.
[45] Bettis, B., Hosder, S., and Winter, T., 2011, "Efficient Uncertainty Quantification in Multidisciplinary Analysis of Reusable Launch Vehicle," AIAA Paper No. 2011-2393.
[46] Eldred, M., 2009, "Recent Advances in Non-Intrusive Polynomial Chaos and Stochastic Collocation Methods for Uncertainty Analysis and Design," AIAA Paper No. 2009-2274.
[47] Hosder, S., Walters, R., and Balch, M., 2008, "Point-Collocation Nonintrusive Polynomial Chaos Method for Stochastic Computational Fluid Dynamics," AIAA J., **53**, pp. 437–465.
[48] Xiu, D., and Karniadakis, G., 2002, "The Wiener-Askey Polynomial Chaos for Stochastic Differential Equations," SIAM J. Sci. Comput., **24**(2), pp. 619–644.
[49] Reddy, S. R., 2019, "Many-Objective Hybrid Optimization Under Uncertainty With Applications," Ph.D. thesis, Florida International University, Miami, FL.
[50] Hosder, S., Walkers, R. W., and Balch, M., 2007, "Efficient Sampling for Non-Intrusive Polynomial Chaos Applications With Multiple Uncertain Input Variables," AIAA Paper No. 2007-1939.
[51] Feinberg, J., and Langtangen, H., 2015, "Chaospy: An Open Source Tool for Designing Method of Uncertainty Quantification," J. Comput. Sci., **11**, pp. 46–57.
[52] Sudret, B., 2008, "Global Sensitivity Analysis Using Polynomial Chaos Expansions," Reliab. Eng. Syst. Saf., **93**(7), pp. 964–979.
[53] Crestaux, T., Le Maître, O. L., and Martinez, J.-M., 2009, "Polynomial Chaos Expansion for Sensitivity Analysis," Reliab. Eng. Syst. Saf., **94**(7), pp. 1161–1172.
[54] Wintzer, M., and Ordaz, I., 2015, "Under-Track CFD-Based Shape Optimization for a Low-Boom Demonstrator Concept," AIAA Paper No. 2015–2260.
[55] Ordaz, I., Wintzer, M., and Rallabhandi, S. K., 2015, "Full-Carpet Design of a Low-Boom Demonstrator Concept," AIAA Paper No. 2015–2261.
[56] Park, M. A., and Nemec, M., 2017, "Near Field Summary and Statistical Analysis of the Second AIAA Sonic Boom Prediction Workshop," AIAA Paper No. 2017–3256.
[57] Carpenter, F. L., Cizmas, P. G., Reddy, S. R., and Dulikravich, G. S., "Controlling Sonic Boom Loudness Through Outer Mold Line Modification: A Sensitivity Study," AIAA Paper No. 2019-0603.